Environmental Science Nano

Accepted Manuscript

ROYAL SOCIETY OF CHEMISTRY

rsc.li/es-nano

Nano Impact Statement

To evaluate the potential for human and ecological exposure to engineered nanomaterials, it is important to consider the impact of stabilizing agents on their environmental fate. This study coupled experimental work with mathematical modeling to investigate the influence of a polymeric sunscreen additive on the transport and deposition behavior of titanium dioxide nanoparticles ($nTiO_2$) in porous media. The transport model was able to predict nanoparticle breakthrough behavior and total retained mass in column experiments, and could be applied in future studies to evaluate different nanomaterials and experimental conditions. The findings demonstrate that the addition of a polymeric sunscreen additive to $nTiO_2$ suspensions could increase their mobility in the environment, increasing the potential for exposure and contamination of drinking water sources.

Influence of a Polymer Sunscreen Additive on the Transport and Retention of Titanium Dioxide Nanoparticles in Water-Saturated Porous Media

Jessica Englehart, Bonnie A. Lyon, Matthew D. Becker[1], Yonggang Wang, Linda M. Abriola, Kurt D. Pennell*

Department of Civil and Environmental Engineering, Tufts University, 200 College Avenue, Medford, Massachusetts 02155, USA

*Corresponding author:

Kurt D. Pennell, PhD, PE, BCEE
Department of Civil & Environmental Engineering
Tufts University
200 College Avenue
Medford, MA 02155
Tel: 617-627-3099
Fax: 617-627-3994
Email: kurt.pennell@tufts.edu

[1]Current address: John and Willie Leone Family Department of Energy and Mineral Engineering and EMS Energy Institute, The Pennsylvania State University, University Park, Pennsylvania 16802, USA

Abstract

Titanium dioxide nanoparticles ($nTiO_2$) are utilized in an array of consumer products including paints, sunscreens, cosmetics, and food. These products typically contain stabilizing agents that may alter $nTiO_2$ fate when released into the environment. The objective of this study was to investigate the effects of TEGO Carbomer, a polymeric stabilizing agent used in sunscreen, on the transport and deposition behavior of TiO_2 nanoparticles in porous media. Aqueous $nTiO_2$ suspensions at pH 5.0 or 7.5±0.2 were introduced into water-saturated columns packed with Federal Fine Ottawa sand. In the absence of Carbomer, $nTiO_2$ was not detected in effluent samples at pH 5, which was below the estimated point of zero charge (PZC) of $nTiO_2$ (pH 6.3), while greater than 80% elution of $nTiO_2$ was observed at pH 7.5. The addition of 3 mg/L Carbomer decreased the PZC from 6.3 to less than 5, and resulted in greater than 94% elution of $nTiO_2$ at pH 5 and 7.5. A nanoparticle transport model that incorporates a first-order, maximum retention capacity term was able to capture column breakthrough and retention data. Model results indicate that the presence of Carbomer reduced the average retention capacity of the solid phase from 3.40 to 1.10 µg TiO_2/g sand, irrespective of solution chemistry changes. These findings demonstrate the substantial impact that polymeric stabilizing agents can have on the fate of $nTiO_2$ in porous media, potentially enhancing $nTiO_2$ mobility in the environment and reducing the efficiency of filtration systems for $nTiO_2$.

Keywords: nano-TiO_2, titanium dioxide, nanoparticle, mobility, transport, polymeric stabilizing agent, sunscreen, Carbomer

1. Introduction

Titanium dioxide (TiO_2) is used in a wide range of consumer products including toothpaste and sunscreen, as a food additive and whitener, and as a pigment in paints, plastics, and paper.[1, 2] Due to the unique and desirable properties of nano-scale TiO_2 ($nTiO_2$), the proportion of nano- versus bulk-TiO_2 production is expected to increase exponentially over the next decade, with an upper estimate of 2.5 million metric tons of $nTiO_2$ produced by 2025.[3] For example, sunscreen manufacturers have demonstrated that by decreasing the primary particle size of TiO_2 in sunscreen formulations, the sun protection factor can be improved while minimizing the undesirable skin whitening effect often imparted by TiO_2-based UV filters.[4]

The widespread use of $nTiO_2$ in consumer products will inevitably lead to direct or indirect releases to the environment. In a study detailing the lifecycle of nTiO2 in sunscreen, Botta et al.[5] found that a substantial amount of $nTiO_2$ residue will disperse into aquatic environments as a result of sunscreen use (up to 30% of the total $nTiO_2$ in the applied sunscreen). Nano-TiO_2 contained in food additives or in cosmetic products and sunscreens that are washed off during bathing or cleaning are likely to enter wastewater treatment plants (WWTPs). A recent study by Weir and colleagues estimated a daily loading rate to sewage systems of 0.1 mg $nTiO_2$/person/day, based on ingestion of $nTiO_2$-containing foods in the United States.[2] Although partial removal of $nTiO_2$ in WWTPs has been reported, concentrations of 5-15 µg/L as Ti have been measured in wastewater effluents,[6, 7] demonstrating that $nTiO_2$ will persist and be discharged after treatment. Furthermore, if WWTP biosolids containing $nTiO_2$ are land applied, additional $nTiO_2$ could enter the environment. Release of part per billion (µg/L) levels of $nTiO_2$ from exterior building paint was shown by Kaegi and colleagues,[8] indicating that urban runoff represents another route for $nTiO_2$ to enter the environment.

TiO_2 has been classified by the International Agency for Research on Cancer (IARC) as a possible human carcinogen, primarily based on health effects resulting from inhalation.[9] $nTiO_2$ ingestion has been linked to Crohn's disease,[10] and prior studies have demonstrated $nTiO_2$ toxicity in human and mammalian cells, as well as ecotoxicity including inhibition of algae growth following exposure to $nTiO_2$.[11, 12] Many factors impact the toxicity of $nTiO_2$,[13-15] including crystalline structure (e.g., rutile vs. anatase),[16] particle coating, and size, but comprehensive physicochemical characterization is often lacking in nanotoxicity studies making it difficult to correlate $nTiO_2$ properties with observed effects.[17] Hence, further research is needed to determine human health impacts and ecological risks associated with $nTiO_2$ in the environment. One critical component of such assessments is a greater understanding of $nTiO_2$ fate and transport under environmentally relevant conditions.

Particle stability and aggregation are important factors in the fate and transport of $nTiO_2$. Jiang et al. found that increasing ionic strength (IS) from 1 to 100 mM NaCl resulted in a 50-fold increase in the hydrodynamic diameter of uncoated $nTiO_2$ with a primary particle size of 15 nm.[18] In the same study, the average $nTiO_2$ size was approximately 90 nm when suspension pH was below 4.2 or above 8.2, at a constant IS of 1 mM. The point of zero charge (PZC) of $nTiO_2$ is reported to range from pH 5.5-6.8,[18-21] and falls within the pH range observed in the aquatic environment.[22] Particle aggregation increases as the pH approaches the PZC, with maximum aggregation occurring at the PZC. In the environment, dissolved natural organic matter (NOM) can stabilize $nTiO_2$ suspensions by reducing particle aggregation, presumably due to steric repulsion.[23] Data presented by Domingos and colleagues suggests that, due to the presence of NOM, $nTiO_2$ dispersion and mobility in the environment may occur to a greater extent than predicted based on prior laboratory experiments.[23] In addition to naturally occurring stabilizing

agents, artificial dispersants are frequently added to nanoparticle suspensions to increase stability and maintain or minimize aggregate size.[24, 25] Joo et al. observed improved $nTiO_2$ suspension stability in the presence of carboxymethyl cellulose (CMC), where suspensions of uncoated $nTiO_2$ exhibited a PZC of 5.6 while CMC-containing $nTiO_2$ suspensions had a PZC of less than 2.[25] An additional study, which evaluated the impact of polyacrylic acid on $nTiO_2$ stability, reported a decrease in the PZC by 0.42-2.08 pH units, depending upon the molecular weight (2,000-120,000 g/mol) and concentration (10-100 mg/L) of added polyacryclic acid.[26]

Petosa and colleagues demonstrated that polymer-coated (partially cross-linked polyacrylic acid) $nTiO_2$ particles had greater mobility in quartz sands compared to bare $nTiO_2$ for IS ranging from 0.1-100 mM as $NaNO_3$.[27] In another study by Joo et al., nearly complete retention of uncoated anatase $nTiO_2$ was reported in quartz sand columns, while the addition of CMC to $nTiO_2$ suspensions ($nTiO_2$:CMC ratio of 0.1:1) resulted in nanoparticle breakthrough after 1 pore volume (PV), which was attributed to electrosteric stabilization from the adsorption of CMC to the nanoparticles.[25] With the exception of a few studies,[24, 25, 27] the majority of previous $nTiO_2$ transport experiments were performed with uncoated $nTiO_2$ or in the absence of stabilizing agents, and did not consider the matrices utilized in most commercial products containing $nTiO_2$. Sunscreens represent a major class of personal care products and potential route of entry for $nTiO_2$ into the environment.[5] Thus, in order to predict the fate of $nTiO_2$, it will be important to understand the influence of specific sunscreen additives on stability and transport in the environment. The stabilizing agents considered in previous $nTiO_2$ transport studies include non-ionic and anionic surfactants[24] carboxymethyl cellulose,[25] and clay particles,[28] but the effect of a specific sunscreen additive has not been evaluated. Additionally, very few prior studies measured the amount of retained $nTiO_2$ (i.e., the solid-phase concentration) in column transport

experiments[28-30] due the difficulties associated with accurately measuring deposited TiO_2 concentrations. Measurement of retained mass, however, is critical to experimental mass balance closure and is also important for transport model validation.

The objective of this research was to investigate the effects of a polymeric stabilizing agent used in sunscreen formulations (Carbomer) on the mobility of TiO_2 nanoparticles in porous media. Batch studies were carried out to determine the effects of pH and IS on the aggregation, particle size distribution, and zeta potential of $nTiO_2$ in the presence and absence of Carbomer. Column experiments were conducted to evaluate the influence of the stabilizing agent on the transport and deposition of $nTiO_2$ in water-saturated quartz sands at pH values of 5.0 and 7.5±0.2. In addition to column effluent samples, $nTiO_2$ solid phase concentrations were measured, allowing for retention profiles and total $nTiO_2$ mass balance to be calculated. A nanoparticle transport model that incorporates a first-order attachment expression and a Langmuirian blocking function was implemented to provide further quantitative interpretation of the experimental results.

2. Materials and methods

2.1. Nanoparticle suspensions

Uncoated TiO_2 nanoparticles (99.5%, Aeroxide TiO_2 P25) and polymeric stabilizing agent (TEGO Carbomer 341 ER) were obtained from the Evonik Degussa Corporation (Essen, Germany). The nominal $nTiO_2$ particle size provided by the manufacturer was 21 nm, with a reported specific surface area of 15 m^2/g and density of 3.8 g/cm^3. The crystalline structure of P25 consists of approximately 78% anatase, 14% rutile, and 8% amorphous TiO_2.[31] The stabilizing agent, TEGO Carbomer 341 ER (hereafter referred to as Carbomer), is an

acrylates/C10-30 alkyl acrylates cross-polymer with a density of 1.4 g/cm^3. The equivalent weight is estimated to be 76 g/mol per carboxyl group,[32] and using an approximate value of 20 carboxyl groups for this compound, the molecular weight was estimated to be 1500 g/mol. A High Protection Sun Lotion recipe from Evonik includes 1.5% (w/w) TEGO Sun T 805 G ($nTiO_2$) and 0.2% (w/w) Carbomer 341, or a 7.5:1 w/w ratio of $nTiO_2$ to Carbomer. In the present study, a similar ratio of these components was used for suspensions containing Carbomer (10:1 w/w).

$nTiO_2$ suspensions were prepared by mixing a pre-weighed mass of dry P25 powder with deionized (DI) water, generating a final suspension concentration of approximately 30 mg/L. Suspension IS was adjusted to values ranging from 0.01-100 mM using 1 M NaCl. Samples were adjusted to pH 5 using 0.1 M HCl, while pH 7.5 samples were buffered with 1 mM HEPES buffer (Acros Organics, New Jersey). For samples containing stabilizing agent, Carbomer was first added to DI water and mixed for ten minutes prior to the addition of nanoparticles, followed by IS and pH adjustment using the same procedure as the samples without stabilizing agent. The final suspensions (including $nTiO_2$) were sonicated for 10 minutes using a Branson Sonifier 450 sonication probe (Branson Ultrasonics, Danbury, CT) with a microtip attachment.

2.2. Nanoparticle characterization

The hydrodynamic diameter and electrophoretic mobility of $nTiO_2$ suspensions were measured with a Malvern ZetaSizer (Malvern, Worcestershire, United Kingdom) using dynamic light scattering (DLS) and laser Doppler velocimetry, respectively. The electrophoretic mobility was then related to the zeta potential (ζ) using the Smoluchowski approximation.[33] The particle size distribution, pH, and zeta potential of the influent suspension were monitored at the

beginning and end of each column experiment. In batch experiments, DLS measurements were taken one minute after NaCl addition to evaluate the impact of ionic strength on $nTiO_2$ size and zeta potential. Solution pH was monitored using an Orion 3 Star pH Benchtop probe (Thermo Scientific, Waltham, MA). The measured pH values of the $nTiO_2$ suspensions used in column transport studies ranged from 5.0-5.2 and 7.4-7.7 (Table 1). Transmission electron microscope (TEM) images of $nTiO_2$ with and without 3 mg/L Carbomer were obtained using a JEOL 2100 TEM (JEOL USA, Peabody, MA) and are shown in the electronic supplementary information, ESI (Figure S1). Samples were prepared by evaporating several drops of 30 mg/L $nTiO_2$ suspensions (at pH 7.5 with 1 mM HEPES buffer) onto a carbon film on 400 square mesh copper grid (Electron Microscopy Sciences, Hatfield, PA).

2.3. Column transport experiments

All column studies were conducted with Federal Fine Ottawa sand (30-140 mesh, d_{50} = 320 µm) which was obtained from the U.S. Silica Company (Ottawa, IL). The sand was cleaned by soaking in 1.0 M HNO_3 solution overnight, rinsing with DI, and was then placed in an ultrasonic bath containing 0.007 M Na_2PO_4 for at least 10 h, rinsed with DI until pH 7 was reached, and finally oven-dried at 200°C for 12 h.[34] Transport experiments were performed using borosilicate glass columns (10 cm length × 2.5 cm inner diameter, Kontes, Vineland, NJ), which were dry-packed with washed Federal Fine Ottawa sand in 1-cm increments. Both end plates of the column contained a 60-mesh stainless steel screen to support the packed bed and prevent elution of sand grains. Once packing was complete, the column was flushed with CO_2 gas for at least 20 minutes to facilitate dissolution of entrapped gas bubbles during water imbibition. A background solution (DI for Columns 1-8 or 3 mM NaCl for Columns 9-12) was then injected into the

column in an upward direction for at least 10 PVs using an ISO-100 Isocratic Pump (Chrom Tech, Apple Valley, MN). Following complete saturation of the column, a non-reactive tracer test was performed to assess water flow and hydrodynamic dispersion within the column. Three PVs of non-reactive tracer solution (1 mM NaBr for Columns 1-8, 3 mM NaBr for Columns 9-12) were injected at a flow rate of 1 mL/min, followed by at least two PVs of background solution. The bromide concentration in aqueous samples was measured using a bromide combination electrode (Cole-Parmer, Vernon Hills, IL). Effluent breakthrough curves (BTCs) obtained for the bromide tracer were fit to a dimensionless form of the advection-reactive transport (ADR) equation for each column using the CXTFIT program.[35] The average column Peclet number was 148±35, which corresponds to a hydrodynamic dispersion coefficient (D_H) of 0.041±0.01 cm^2/min. A representative model fit to a measured tracer breakthrough curve is shown in Figure 6.

Following the tracer test, a three PV pulse of $nTiO_2$ suspension was injected into the column using a PHD 2000 syringe pump (Harvard Apparatus, Holliston, MA) at a flow rate of 1 mL/min, followed by at least two PVs of $nTiO_2$-free background electrolyte solution, also at a flow rate of 1 mL/min. The average Darcy velocity of background electrolyte and $nTiO_2$ injections was 2.8±0.06 m/d, corresponding to an average pore-water velocity of 7.3±0.3 m/d. This value is similar to the seepage velocity used by Cai et al. (8 m/d) in a previous $nTiO_2$ transport study[28] to represent flow through coarse aquifer sediments or engineered filtration systems. Column effluent samples were collected continuously (at least five samples per PV) using a Spectrum Labs Spectra/Chrom CF-2 Fraction Collector (Spectrum Laboratories, Inc., Rancho Dominguez, CA). Columns 1-8 were run with a DI water background to first evaluate the role of pH and Carbomer addition, and then the effect of background electrolyte (3 mM

NaCl) in the presence of Carbomer was investigated (Columns 9-12). After each experiment, the columns were sectioned into ten 1-cm increments and approximately 2 g of sand from each increment was analyzed to determine the amount of retained $nTiO_2$.

Column effluent and solid samples were oven-dried at 90°C and then digested in 18.7 M sulfuric acid (2 mL H_2SO_4 for aqueous samples, 5 mL for solid samples) with a CEM SP-D Discover Microwave Digester (CEM Corporation, Matthews, NC). Acid digestion was conducted at 200°C for 45 minutes for aqueous samples and 200°C for 60 minutes for solid samples. After digestion, the samples were diluted to 1 M H_2SO_4 using DI water and quantified using an Optima 7300 DV Inductively Coupled Plasma Optical Emission Spectrometer, ICP-OES (PerkinElmer, Waltham, MA). Standard curves were prepared from an Ultima Titanium stock standard (1,000 mg/L). The average background titanium concentration of the cleaned Federal Fine Ottawa Sand was 18 µg TiO_2/g sand. Titanium was quantified at a wavelength of 336.121 nm, which yielded a detection limit of 12 µg Ti/L (equivalent to 20 µg TiO_2/L), based on the U.S. Environmental Protection Agency method for determining a lowest concentration minimum reporting level.[36]

2.4. Mathematical modeling

The transport of $nTiO_2$ in the homogeneous saturated packed column can be described by a one-dimensional mass balance equation with first-order particle retention kinetics:[34, 37]

$$\frac{\partial C}{\partial t} + \frac{\rho_b}{n}\frac{\partial S}{\partial t} = D_H \frac{\partial^2 C}{\partial x^2} - v_p \frac{\partial C}{\partial x} \quad (1)$$

$$\frac{\rho_b}{n}\frac{\partial S}{\partial t} = k_{att} \Psi C \quad (2)$$

where C is the aqueous phase concentration of suspended particles [M/L^3], t is time [T], k_{att} is the first-order particle attachment rate [T^{-1}], D_H is the hydrodynamic dispersion coefficient [L^2/T], x is the distance from the column inlet [L], v_p is the pore water velocity [L/T], ρ_b is the bulk density [M/L^3], n is the bed porosity [-], which is equivalent to the volumetric water content in saturated media, and S is the concentration of attached particles [M/M]. In this modified first-order model, Ψ [-] is a Langmuirian blocking function that is expressed by:[34]

$$\Psi = \frac{S_{max} - S}{S_{max}} \quad (3)$$

where S_{max} is the maximum retention capacity for $nTiO_2$ on the sand, a system-specific parameter that is associated with the available area for nanoparticle attachment. Here, Ψ is a spatiotemporal function of the retained $nTiO_2$ concentration that decreases from unity to zero as the attached concentration, S, approaches the maximum retention capacity, S_{max}.

Equations 1–3 were solved with an implicit-in-time and central-in-space finite difference scheme implemented in MATLAB R2010a (The Mathworks Inc., Natick, MA). Pore-water velocity, v_p, and hydrodynamic dispersion, D_H, terms were independently determined from column tracer data. k_{att} and S_{max} were then determined by fitting the model to effluent breakthrough data using a non-linear least squares minimization algorithm.[38] The transport model (with zero attachment) was also validated against the tracer data fit (that was performed using the CXTFIT program)[35] to confirm that it appropriately captured hydrodynamic dispersion.

3. Results and discussion

3.1. Characterization of nTiO2 suspensions

Batch studies were performed to evaluate the effects of solution pH and IS on the zeta potential and mean diameter of $nTiO_2$. By varying the suspension pH from 3.5-11.5 in DI water,

the PZC of $nTiO_2$ was estimated to be pH 6.3 (Figure 1). This value is comparable to the $nTiO_2$ PZC reported in previous studies; 6.0,[18] 6.8,[20] and 6.2.[30] The $nTiO_2$ zeta potentials ranged from +36.5 to -48.3 mV over the pH range of 3.5-11.5, with positive zeta potentials for pH values below the PZC and negative zeta potentials for pH values above the PZC. Within one pH unit of the PZC, $nTiO_2$ particles aggregated to become micron-sized (mean $nTiO_2$ diameter = 1.31±0.2 μm for pH 5.7-7.0 in DI water, Figure 1). The particle size remained below 150 nm when the pH was at least one unit above or below the PZC. Over the pH range of 3.5-4.7, the average particle diameter was 122±21 nm, and for pH values of 7.8-11.5, the average particle diameter was 103±24 nm (Figure 1).

The influence of IS (0.01-10 mM) on the mean particle diameter and zeta potential of $nTiO_2$ suspensions without stabilizing agent at pH 5 and 7.5 is shown in Figure 2. As expected, the nanoparticles were highly sensitive to changes in solution chemistry in the absence of a stabilizing agent. At pH 5, an increase in $nTiO_2$ particle diameter compared to that in DI water was observed at NaCl concentrations as low as 0.1 mM. When the IS was further increased to 1 mM NaCl, the particle diameter increased more than two-fold (288±50 nm) compared to its value in DI water (112±17 nm). At IS values ≥5 mM NaCl and pH 5, the $nTiO_2$ suspension became unstable, resulting in sedimentation of larger nanoparticle aggregates, and, therefore, unstable size distribution and zeta potential readings. In a previous study using 100% anatase $nTiO_2$ at pH 4.6, Jiang et al. observed a similar trend of increasing $nTiO_2$ size and with increasing IS, with substantial aggregation occurring at IS values of 5 mM NaCl and higher.[18] In contrast to pH 5 samples, the zeta potential of $nTiO_2$ at pH 7.5 remained relatively constant even when the IS was increased from 0.01 to 10 mM NaCl (mean zeta potential = -22±2.1 mV) in the present study. Although the zeta potential remained stable in pH 7.5 suspensions, particle

aggregation was observed and micron-sized aggregates began to form between IS values of 1 mM and 5 mM NaCl.

The addition of 3 mg/L Carbomer to $nTiO_2$ suspensions resulted in stable particle size and zeta potential for IS values ranging from 0.01 to 100 mM, effectively mitigating the pH effects observed in the absence of Carbomer (Figure 3). At a Carbomer concentration of 3 mg/L, the mean $nTiO_2$ diameter over the entire range of IS was 124±37 nm and 117±37 nm at pH 5 and 7.5, respectively, and the average zeta potential was -42±2 mV and -37±4 mV at pH 5 and 7.5, respectively. The observed differences in mean $nTiO_2$ diameters across IS values were not statistically significant (paired two-tailed t-test, $\alpha = 0.05$, p-value = 0.50), even though the mean zeta potential values were significantly different (p-value <0.01). The enhanced stability of nTiO2 suspensions that was observed following the addition of Carbomer was likely due to electrosteric repulsion resulting from adsorption of the polymer to the $nTiO_2$ surface. A previous study by Liufu et al. demonstrated that adsorption of polyacrylic acid on $nTiO_2$ occurs by hydrogen bonding and chemical interaction between the TiO_2 surface and carboxyl groups of the polymer, which stabilizes $nTiO_2$ suspensions through electrosteric repulsion.[26]

3.2. DLVO energy profiles: nanoparticle-nanoparticle interactions

To qualitatively examine the effects of IS on $nTiO_2$ aggregation, Derjaguin-Landau-Verwey-Overbeek (DLVO) interaction energy profiles were calculated for two spherical TiO_2 nanoparticles (see ESI for equations used). For $nTiO_2$ suspensions without a stabilizing agent, the magnitude of the primary energy barrier decreased with increasing IS (ESI, Figure S2). For pH 5 suspensions with 0.1 mM NaCl, a repulsive energy barrier existed between two approaching TiO_2 nanoparticles (net positive interaction energy). At IS values of 1 mM or higher, a net negative interaction energy was computed, indicating that $nTiO_2$ particles would be

attracted to one another. The computed interaction energy profiles were consistent with the observed increase in $nTiO_2$ particle size when the IS was increased above 1 mM (Figure 2). The interaction energy profiles for an $nTiO_2$ suspension at pH 7.5 were similar to those obtained at pH 5; however, the maximum energy values were slightly higher at pH 7.5 (16.2 versus 14.8 kT at 0.01 mM), and there was a slight repulsive energy at an IS of 1 mM that was not observed at pH 5. Thus, the DLVO interaction energy profiles were consistent with the batch experiment results; specifically, the pH 7.5 suspension was less sensitive to increasing IS, and $nTiO_2$ aggregation was initiated at higher electrolyte concentrations at pH 7.5 compared to pH 5. The primary energy barriers calculated here were on the same order of magnitude as those calculated by Chen et al. (i.e., 10-100 kT).[29]

Traditional DLVO theory does not account for enhanced stability of nanoparticles resulting from the presence of polymers such as Carbomer. Therefore, extended DLVO (XDLVO) was used to compute interaction energy profiles for suspensions containing Carbomer (Figure 4). In XDLVO, the total interaction energy includes not only the traditional electronic double layer repulsive energy and van der Waals attractive energy, but also the osmotic and elastic-steric repulsion energies induced by the presence of a polymer layer coating a colloid or nanoparticle.[39] The equations and parameters used for XDLVO calculations are provided in ESI (Table S1). The repulsive energy barriers based on XDLVO calculations reached maximum values of >20,000 kT at pH 5 and 7.5 for IS values of 0.01-100 mM (Figure 4, inset). The large primary energy barrier exists within the region of the polymer layer surrounding the particle (d = 0-10 nm), and the repulsive force is primarily due to elastic-steric forces. At both pH 5 and pH 7.5, a secondary energy minimum is observed at IS values of 10 and 100 mM, indicating that, although there is large repulsive energy barrier, attractive forces do exist with higher IS solutions. In

comparison, the primary energy barriers obtained using traditional DLVO theory for $nTiO_2$ with Carbomer were higher than those obtained for $nTiO_2$ alone (e.g., 63 kT with Carbomer versus 15 kT without Carbomer at pH 5 and IS = 0.01 mM, ESI Figures S2 and S3), but were several orders of magnitude lower than those obtained using XDLVO theory.

3.3. DLVO energy profiles: nanoparticle-sand surface interactions

Consideration of interaction energy profiles between an $nTiO_2$ particle and a quartz surface provides a qualitative understanding of the potential for nanoparticle deposition during transport through porous media. Energy profiles obtained using DLVO theory for a spherical $nTiO_2$ particle and a quartz surface (represented as a plane) are shown in ESI Figure S4 (calculations provided in ESI). At pH 5, the energy profiles are dominated by a net attractive energy. In contrast, the pH 7.5 profiles indicate positive (repulsive) interaction energies between $nTiO_2$ and the quartz surface (ESI Figure S4). At pH 7.5 and 10 mM NaCl, a secondary energy minimum occurs at a separation distance of 16.2 nm, indicating that although there is a repulsive primary energy barrier, attractive forces exist between $nTiO_2$ and the quartz surface, which may contribute to deposition under these conditions.

To evaluate the impact of steric repulsion on interaction energy in the presence of a polymer, XDLVO theory was applied to the nanoparticle-quartz surface system.[40, 41] For this case, the steric interaction energy was calculated between a polymer-coated TiO_2 nanoparticle and an uncoated sand grain and summed with the nanoparticle-sand grain electronic double layer repulsive energy and van der Waals attractive energy to obtain the total interaction energy (Figure 5, see ESI for equations). The inclusion of steric energy in the XDLVO calculation results in a large positive (repulsive) energy in the region of the polymer layer 0-10 nm from the

particle surface, which is consistent with the stabilization of $nTiO_2$ due to an adsorbed polymer coating. In contrast to the interaction energy profiles for $nTiO_2$ and quartz sand in the absence of Carbomer (ESI, Figure S4), repulsive forces dominate for both pH 5 and 7.5 at low IS (≤1 mM NaCl) when Carbomer was present (Figure 5). Dominant repulsive forces suggest that under these conditions, $nTiO_2$ will not be deposited on porous media, and therefore, the mobility of pH 5 $nTiO_2$ suspensions is expected to be enhanced by the presence of Carbomer. For higher IS suspensions (≥10 mM NaCl), a secondary minimum attractive energy was obtained even though a large primary energy barrier existed due to steric repulsion. A similar trend was observed in XDLVO profiles presented by Wang et al. for polyacryclic acid-octylamine-coated quantum dots, with secondary energy minimums observed at IS values of 30 and 100 mM NaCl.[42]

3.4. Column transport experiments

Results of the column transport studies are presented in two parts; $nTiO_2$ effluent BTCs and solid phase retention profiles. The BTCs are plotted as the measured concentration of $nTiO_2$ in effluent samples (C), divided by the influent or applied concentration (C_0), versus time, expressed as dimensionless PVs. For each column study, the BTC obtained for a pulse injection of non-reactive tracer is shown as a dashed line for comparison purposes. The retention profiles show the concentration of attached $nTiO_2$ (i.e., solid-phase concentration) as a function of distance from the column inlet (x = 0). Measured $nTiO_2$ effluent BTCs and retention profiles in the presence and absence of Carbomer at both pH values are shown in Figures 6-9. Results obtained for column studies conducted with an IS of 3 mM (NaCl) at both pH values are provided in ESI (Figures S5-S6). Experimental conditions for all of the column studies are summarized in Table 1.

365

366 **3.4.1. Mobility of $nTiO_2$ alone**

367 In the absence of Carbomer, there was no measurable breakthrough of $nTiO_2$ in duplicate
368 column experiments performed at pH 5 (Columns 1-2, Figure 6). A maximum solid-phase
369 concentration of 76 μg TiO_2/g sand was measured near the column inlet, which decreased
370 exponentially with travel distance from the inlet. In contrast, when the pH was increased to 7.4,
371 which is above the PZC, 82-90% of the injected $nTiO_2$ mass was recovered in the column
372 effluent (Columns 3-4, Figure 7). The $nTiO_2$ retention profile obtained at pH 7.4 exhibited a
373 gradual decrease in solid-phase concentration along the length of the column, with a maximum
374 value of 6.2 μg TiO_2/g sand occurring at the column inlet. Influent particle diameters of $nTiO_2$
375 were similar in pH 5 and pH 7.4 suspensions (average = 118 nm and 120 nm, respectively),
376 however, the $nTiO_2$ zeta potential was positive (average ζ= +17 mV) at pH 5 and negative at pH
377 7.4 (average ζ= -25 mV). Thus, the difference in surface charge (i.e., zeta potential) was directly
378 related to the mobility of $nTiO_2$ in Federal Fine sand; particles with positive zeta potentials were
379 completely retained (0% breakthrough), while particles with negative zeta potentials exhibited
380 greater than 82% mass breakthrough. These findings are consistent with the PZC data and
381 DLVO interaction energy profiles discussed above. A previous study also reported complete
382 retention of uncoated $nTiO_2$ at pH 5.5, which was near the PZC calculated in that study (pH =
383 5.6).[25] However, in that case, deposition was attributed to instability and aggregation of the
384 $nTiO_2$ suspension (average hydrodynamic diameter = 753 nm).

385

386 **3.4.2. Mobility of $nTiO_2$ in the presence of Carbomer**

The addition of 3 mg/L Carbomer to $nTiO_2$ suspensions resulted in nearly complete breakthrough (94-104%) of the applied $nTiO_2$ mass at both pH 5.1 and 7.6 (Columns 5-8, Figures 8 and 9). At pH 5.1 and 7.6, the measured $nTiO_2$ effluent BTCs were similar, although the maximum $nTiO_2$ retention at pH 7.6 was substantially greater than the retention observed at pH 5.1 (5.8 vs. 0.9 μg TiO_2/g sand). However, $nTiO_2$ retention was only detected in the 2 cm nearest the column inlet and accounted for less than 6% of the applied mass (Figures 8 and 9); at all other locations along the length of the column $nTiO_2$ retention was below the detection limit (<0.86 μg TiO_2/g sand). Thus, Carbomer addition mitigated the effect of pH on $nTiO_2$ that was observed in its absence (i.e., complete retention at pH 5.1), which is consistent with the nanoparticle-sand DLVO and XDLVO interaction energy profiles (i.e., Figure S4 vs. Figure 5).

When 3 mM NaCl was added to Carbomer-$nTiO_2$ suspensions at pH 5.2 and pH 7.7 (Columns 9-12, Figures S5-S6), there was minimal change in $nTiO_2$ mobility (<8% change in mass breakthrough) compared to identical column studies performed without NaCl (Columns 5-8, Figures 8 and 9). This finding was consistent with the XDLVO theory, which indicated that $nTiO_2$ particle-particle and particle-surface interaction energy profiles were not sensitive to low electrolyte concentrations in the presence of Carbomer (Figures 4 and 5). Similar to the trend observed for column experiments conducted in the presence of Carbomer without NaCl (Columns 5-8), the $nTiO_2$ effluent BTC obtained at pH 7.7 with 3 mg/L Carbomer and 3 mM NaCl (Columns 11-12) rose more slowly than the $nTiO_2$ BTC obtained at pH 5.2 under the same conditions (Columns 9-10). No measurable $nTiO_2$ retention was observed at pH 5.2, while the solid phase sample collected nearest the column inlet yielded concentrations of 4.8 and 3.0 μg TiO_2/g sand in replicate experiments conducted at pH 7.7. Zeta potential values obtained in the presence of Carbomer were negative at pH 5-5.2, indicating that the PZC shifted to a pH value

lower than 5. Joo et al. observed a similar decrease in the PZC (from pH 5.6 to <2) and enhanced $nTiO_2$ mobility through quartz sand following addition of a different polymer stabilizing agent (carboxymethyl cellulose, MW = 90,000 g/mol) to $nTiO_2$ suspensions.[25]

3.4.3. Mathematical modeling results

At pH 5.0 in DI water (Columns 1 and 2), $nTiO_2$ exhibited a positive zeta potential (Table 1), and thus, the retention capacity on the negatively charged sand surface (sand zeta potential = -35 mV)[43] was very large relative to the injected concentration (i.e., $S_{max} \rightarrow \infty$), reducing the attachment term in the model to a constant first-order expression (i.e., $\Psi = 1$ for all space and time). For Columns 3-12, the nanoparticle transport model described by Equations 1-3 was fit to effluent BTC data to obtain k_{att} and S_{max} values for each experiment (Table 1). Retention profiles were then predicted from the model fits. The model captured the slow rise to a steady-state concentration plateau (e.g., see Figure 9a), behavior that cannot be described using a traditional constant first-order particle deposition model.[34] With the exception of Columns 1 and 2, fitted k_{att} values fell within one order-of-magnitude of each other (average $k_{att} = 3.61\times10^{-4}$ s^{-1}), consistent with the similarity in $nTiO_2$ zeta potential values measured under these conditions. Fitted k_{att} values for Columns 1 and 2 were an order of magnitude larger (average $k_{att} = 3.85 \times 10^{-3}$ s^{-1}), a consequence of the higher affinity between the positively-charged $nTiO_2$ and the negatively-charged sand surface. A recent study by Toloni et al.[37] reported a similar attachment rate ($k_{att} = 1.3\times10^{-3}$ s^{-1}) for $nTiO_2$ transport in quartz sand at a pore-water velocity of 10 m/day, but did not consider the impact of polymers or stabilizing agents on model rate parameters. In the present study, the addition of Carbomer resulted in a ca. 3-fold decrease in S_{max} (average S_{max}

= 3.40 μg TiO_2/g sand for Columns 3 and 4; 1.10 μg TiO_2/g sand for Columns 5-12), regardless of pH and IS.

Collision efficiency (α) values were calculated from the fitted k_{att} values using clean-bed filtration theory:[44]

$$\alpha = \frac{2d_{50}}{3(1-n)\eta_0 L} k_{att} \quad (4)$$

where d_{50} is the median sand grain size [L], L is the length of the packed column [L], and η_0 is the single-collector contact efficiency. In theory, three mechanisms contribute to η_0: Brownian diffusion (η_D), interception (η_I), and gravitational sedimentation (η_G).[44] Correlations for each value (η_D, η_I, and η_G) developed by Tufenkji and Elimelech[45] were used to estimate the attachment efficiency, α, for TiO_2 on the sand surface from the fitted attachment rate (equations provided in ESI). In Columns 3-12, α values ranged from 0.010 to 0.065, consistent with the unfavorable conditions for nanoparticle attachment in those experiments. In Columns 1 and 2 however, α was 0.32, indicating much more favorable conditions for nanoparticle attachment, consistent with energy profiles obtained from DLVO theory (ESI, Figure S4a). Collision efficiency values associated with the addition of Carbomer (Columns 5-12) were not substantially different from those fitted to the Carbomer-free experiments at pH 5 (Columns 3 and 4), indicating that the polymer did not influence the attachment efficiency of $nTiO_2$ particles under these conditions. This result suggests that the change in $nTiO_2$ retention in columns with added Carbomer was caused by a decrease in the surface area available for $nTiO_2$ attachment rather than alteration of attachment kinetics.

Although the breakthrough behavior was well captured in all cases, the model based upon equations 1-2 with a single (average) S_{max} value was unable to accurately reproduce the hyper-exponential retention curves exhibited in Columns 3-12 (see, for example, Figure 9b). Although

models for mechanical filtration (i.e., straining) of colloidal particles in porous media predict hyper-exponential retention behavior, the measured particle sizes observed in this study were approximately 120 nm, resulting in $nTiO_2$ to porous media diameter (d_{50} = 350 µm) ratios ranging from 3.0×10^{-4} to 3.9×10^{-4}. Typically, straining is considered to be significant when the ratio of particle diameter to grain diameter is greater than 0.05,[46] although more recent studies have suggested that straining may be a factor at ratios of 0.002 or 0.008.[47, 48] Since the nanoparticle:grain size diameter ratio were an order of magnitude lower than the reported threshold values, it is unlikely that physical straining contributed to the observed $nTiO_2$ retention. Although the shape of the retention curves was not fully captured, the single-S_{max} retention model was able to accurately capture the total amount of retained mass in all cases. This result suggests that the maximum capacity for $nTiO_2$ retention varied along the domain, but could be represented by a single average retention parameter.

4. Conclusions

The effects of a polymer stabilizing agent, Carbomer (a common sunscreen additive), on the transport and retention behavior of $nTiO_2$ in Federal Fine Ottawa sand was investigated using a combination of experimental and mathematical modeling studies. In the absence of Carbomer, $nTiO_2$ particles aggregated to become micron-sized within one pH unit of the PZC (pH 6.3). The mean diameter of $nTiO_2$ remained below 150 nm when the pH was at least one unit above or below the PZC (size = 122±21 nm and 103±24 nm, for pH ranges of 3.5-4.7 and 7.8-11.5, respectively). The porous medium possessed a negative zeta potential (e.g., estimated to be -35 mV at pH 5),[43] and therefore, when the suspension pH was below the PZC (positive $nTiO_2$ zeta potential), limited TiO_2 transport and substantial retention was observed. Conversely, when the

suspension pH was above the PZC (negative $nTiO_2$ zeta potential), $nTiO_2$ was not deposited on the negatively charged quartz surfaces, and thus, mobility increased, demonstrating the important role of pH on $nTiO_2$ mobility in the absence of Carbomer. When $nTiO_2$ suspensions were amended with 3 mg/L Carbomer, zeta potential values were negative at pH 5-5.2, indicating that the PZC shifted to a pH value lower than 5. Since this PZC is less than the pH range typically observed in environment systems (i.e., 6-9)[22], it is expected that $nTiO_2$ particles will exhibit greater mobility in the presence of stabilizing agents.

In the presence of 3 mg/L Carbomer, greater than 94% effluent mass breakthrough occurred in $nTiO_2$ suspensions, regardless of suspension pH or electrolyte content. The enhanced stability of $nTiO_2$ suspensions following Carbomer addition was likely due to increased electrosteric repulsion resulting from adsorption of the polymer to the nanoparticle surface. As a result, the effects of solution pH were overshadowed by the addition of a polymer to $nTiO_2$ suspensions. Simulation of experimental BTCs and retention profiles using a nanoparticle transport model with a first-order kinetic attachment expression and a maximum attachment capacity term adequately described the breakthrough behavior as well as the total amount of retained mass measured in all experiments. However, the model was unable to capture the hyper-exponential $nTiO_2$ retention observed near the column inlet, indicating that there is likely a spatially-variable retention capacity that was not accounted for by the model.

The findings of this study demonstrate the importance of considering the impacts of polymer stabilizing agents on the environmental fate of manufactured TiO_2 nanomaterials that are released into the environment from sunscreen and other consumer products containing a dispersing agent in their formulation. More specifically, the addition of product-relevant concentrations of Carbomer could alter the system retention capacity substantially, thereby

allowing for increased $nTiO_2$ mobility through porous media. Such enhanced transport through porous media or filtration systems could increase the potential for contamination of drinking water sources and risk of human and ecological exposure.

Acknowledgements

Support for this research was provided by grants from the National Science Foundation, Award numbers CBET-0854136 and CBET-1235563. The work has not been subject to NSF review, and therefore, does not necessarily reflect the views of the organization and no official endorsement should be inferred. TEM imaging was performed at the Center for Nanoscale Systems (CNS), a member of the National Nanotechnology Infrastructure Network (NNIN), which is supported by the National Science Foundation under NSF award no. ECS-0335765. CNS is part of Harvard University.

Electronic supplementary information (ESI) available: TEM images; DLVO/XDLVO calculations and parameters; additional transport model equations; DLVO interaction profiles for two $nTiO_2$ particles and for $nTiO_2$-sand grains; BTCs and retention profiles for $nTiO_2$ in the presence of Carbomer and 3 mM NaCl.

References

1. ICIS, ICIS Titanium Dioxide Uses and Market, http://www.icis.com/resources/news/2007/11/07/9076546/titanium-dioxide-tio2-uses-and-market-data/, Accessed February 10, 2014.

2. A. Weir, P. Westerhoff, L. Fabricius, K. Hristovski and N. von Goetz, *Environ. Sci. Technol.*, 2012, **46**, 2242-2250.

3. C. O. Robichaud, A. E. Uyar, M. R. Darby, L. G. Zucker and M. R. Wiesner, *Environ. Sci. Technol.*, 2009, **43**, 4227-4233.

4. S. Wiechers, P. Biehl, C. Luven, M. Maier, J. Meyer, J. Munzenburg, C. Schulze-Isfort and P. Albers, *Cosmet. Toiletries*, 2013, **128**, 332-339.

5. C. Botta, J. Labille, M. Auffan, D. Borschneck, H. Miche, M. Cabié, A. Masion, J. Rose and J.-Y. Bottero, *Environ. Pollut.*, 2011, **159**, 1543-1550.

6. M. A. Kiser, P. Westerhoff, T. Benn, Y. Wang, J. Pérez-Rivera and K. Hristovski, *Environ. Sci. Technol.*, 2009, **43**, 6757-6763.

7. P. Westerhoff, G. Song, K. Hristovski and M. A. Kiser, *J. Environ. Monit.*, 2011, **13**, 1195-1203.

8. R. Kaegi, A. Ulrich, B. Sinnet, R. Vonbank, A. Wichser, S. Zuleeg, H. Simmler, S. Brunner, H. Vonmont, M. Burkhardt and M. Boller, *Environ. Pollut.*, 2008, **156**, 233-239.

9. IARC, *IARC Monographs on the Evaluation of Carcinogenic Risks to Humans: Carbon Black, Titanium Dioxide, and Talc*, International Agency for Research on Cancer, Lyon, France, 2010.

10. M. C. E. Lomer, R. P. H. Thompson and J. J. Powell, *Proc. Nutr. Soc.*, 2002, **61**, 123-130.

11. V. Aruoja, H.-C. Dubourguier, K. Kasemets and A. Kahru, *Sci. Total Environ.*, 2009, **407**, 1461-1468.

12. N. B. Hartmann, F. Von der Kammer, T. Hofmann, M. Baalousha, S. Ottofuelling and A. Baun, *Toxicology*, 2010, **269**, 190-197.

13. G. Frenzilli, M. Bernardeschi, P. Guidi, V. Scarcelli, P. Lucchesi, L. Marsili, M. C. Fossi, A. Brunelli, G. Pojana, A. Marcomini and M. Nigro, *Mar. Environ. Res.*, 2014, **100**, 68-73.

14. S. Huang, P. J. Chueh, Y.-W. Lin, T.-S. Shih and S.-M. Chuang, *Toxicol. Appl. Pharmacol.*, 2009, **241**, 182-194.

15. C.-Y. Jin, B.-S. Zhu, X.-F. Wang and Q.-H. Lu, *Chem. Res. Toxicol.*, 2008, **21**, 1871-1877.

16. C. M. Sayes, R. Wahi, P. A. Kurian, Y. Liu, J. L. West, K. D. Ausman, D. B. Warheit and V. L. Colvin, *Toxicol. Sci.*, 2006, **92**, 174-185.

17. A. Menard, D. Drobne and A. Jemec, *Environ. Pollut.*, 2011, **159**, 677-684.

18. J. Jiang, G. Oberdörster and P. Biswas, *J. Nanopart. Res.*, 2009, **11**, 77-89.

19. K. A. Dunphy Guzman, M. P. Finnegan and J. F. Banfield, *Environ. Sci. Technol.*, 2006, **40**, 7688-7693.

20. R. A. French, A. R. Jacobson, B. Kim, S. L. Isley, R. L. Penn and P. C. Baveye, *Environ. Sci. Technol.*, 2009, **43**, 1354-1359.

21. N. Solovitch, J. Labille, J. Rose, P. Chaurand, D. Borschneck, M. R. Wiesner and J.-Y. Bottero, *Environ. Sci. Technol.*, 2010, **44**, 4897-4902.

22. W. Stumm and J. J. Morgan, *Aquatic Chemistry*, John Wiley & Sons, New York, 3rd edn., 1995.

23. R. F. Domingos, N. Tufenkji and K. J. Wilkinson, *Environ. Sci. Technol.*, 2009, **43**, 1282-1286.

24. I. G. Godinez and C. J. G. Darnault, *Water Res.*, 2011, **45**, 839-851.

25. S. H. Joo, S. R. Al-Abed and T. Luxton, *Environ. Sci. Technol.*, 2009, **43**, 4954-4959.

26. S. Liufu, H. Xiao and Y. Li, *J. Colloid Interf. Sci.*, 2005, **281**, 155-163.

27. A. R. Petosa, S. J. Brennan, F. Rajput and N. Tufenkji, *Water Res.*, 2012, **46**, 1273-1285.

28. L. Cai, M. Tong, X. Wang and H. Kim, *Environ. Sci. Technol.*, 2014, **48**, 7323-7332.

29. G. Chen, X. Liu and C. Su, *Langmuir*, 2011, **27**, 5393-5402.

30. I. Chowdhury, Y. Hong, R. J. Honda and S. L. Walker, *J. Colloid Interf. Sci.*, 2011, **360**, 548-555.

31. B. Ohtani, O. O. Prieto-Mahaney, D. Li and R. Abe, *J. Photoch. Photobio. A*, 2010, **216**, 179-182.

32. B. Goodrich, *BF Goodrich Company Technical Literature: Carbopol Resin Handbook*, 1991.

33. R. J. Hunter, *Zeta Potential in Colloid Science*, Academic Press, New York, 1981.

34. Y. Wang, Y. Li, J. Fortner, J. B. Hughes, L. M. Abriola and K. D. Pennell, *Environ. Sci. Technol.*, 2008, **42**, 3588–3594.

35. N. Toride, F. J. Leij and M. T. van Genuchten, *The CXTFIT code for estimating trnasport parameters from laboratory or field tracer experiments*, U.S. Salinity Laboratory, Agricultural Research Service, U.S. Department of Agriculture, Riverside, CA, 1995.

36. USEPA, *Statistical Protocol for the Determination of the Single-Laboratory Lowest Concentration Minimum Reporting Level (LCMRL) and Validation of Laboratory Performance at or Below the Minimum Reporting Level (MRL)*, Office of Ground Water and Drinking Water, Standards and Risk Management Division, Cincinnati, OH, 2004.

37. I. Toloni, F. Lehmann and P. Ackerer, *J. Contam. Hydrol.*, 2014, **171**, 42-48.

38. M. D. Becker, Y. Wang, K. D. Pennell and L. M. Abriola, *Environ. Sci. Nano*, 2015, **2**, 155-166.

39. G. Fritz, V. Schädler, N. Willenbacher and N. J. Wagner, *Langmuir*, 2002, **18**, 6381-6390.

40. T. L. Byrd and J. Y. Walz, *Environ. Sci. Technol.*, 2005, **39**, 9574-9582.

41. A. R. Petosa, D. P. Jaisi, I. R. Quevedo, M. Elimelech and N. Tufenkji, *Environ. Sci. Technol.*, 2010, **44**, 6532-6549.

42. Y. Wang, H. Zhu, M. D. Becker, J. Englehart, L. M. Abriola, V. L. Colvin and K. D. Pennell, *J. Nanopart. Res.*, 2013, **15**, 1805.

43. A. Kaya and Y. Yukselen, *Canadian Geotechnical Journal*, 2005, **42**, 1280-1289.

44. K. Yao, M. T. Mohammad T. Habibian and C. R. O'Melia, *Environ. Sci. Technol.*, 1971, **5**, 1105-1112.

45. N. Tufenkji and M. Elimelech, *Environ. Sci. Technol.*, 2004, **38**, 529-536.

46. R. Sakthivadivel, *Theory and mechanism of filtration of non-colloidal fines through a porous medium*, Hydraulic Engineering Lab, University of California Berkeley, 1966.

47. X. Li, T. D. Scheibe and W. P. Johnson, *Environ. Sci. Technol.*, 2004, **38**, 5616-5625.

48. S. Xu, B. Gao and J. E. Saiers, *Water Resour. Res.*, 2006, **42**, W12S16.

608 **Table 1.** Summary of experimental conditions and results for column transport studies conducted in Federal Fine (30-140 mesh)
609 Ottawa sand.

	Experimentally Determined Parameters									Mathematical Model Fitted Parameters		
Column ID	**pH**	**Suspension additives**	**C_0[a] (mg $nTiO_2$/L)**	**Porosity (unitless)**	**v_p[b] (m/d)**	**Mass breakthrough (%)**	**Mass balance (%)**	**Particle diameter[c] (nm)**	**Zeta potential (mV)**	**k_{att}[d] (1/s)**	**α[e] (unitless)**	**S_{max}[f] (µg TiO_2/g sand)**
1	5.0	None	24	0.38	7.1	0	85	119	11	3.63×10^{-3}	0.32	n/a
2	5.0	None	24	0.36	7.8	0	84	116	23	4.06×10^{-3}	0.32	n/a
3	7.4	1 mM HEPES	28	0.38	7.1	90	98	107	-28	2.69×10^{-4}	0.022	2.51
4	7.4	1 mM HEPES	29	0.39	7.3	82	93	132	-21	5.95×10^{-4}	0.059	4.28
5	5.1	3 mg/L Carbomer	28	0.37	7.3	104	104	108	-32	4.08×10^{-4}	0.031	0.34
6	5.1	3 mg/L Carbomer	28	0.38	7.4	97	97	109	-36	1.25×10^{-4}	0.010	1.32
7	7.6	1 mM HEPES 3 mg/L Carbomer	32	0.38	7.1	100	103	112	-27	3.61×10^{-4}	0.031	0.78
8	7.6	1 mM HEPES 3 mg/L Carbomer	32	0.38	7.5	94	98	105	-36	4.50×10^{-4}	0.036	1.82
9	5.2	3 mg/L Carbomer 3 mM NaCl	24	0.38	7.2	98	98	129	-50	1.19×10^{-4}	0.012	0.96
10	5.2	3 mg/L Carbomer 3 mM NaCl	25	0.36	7.8	96	96	135	-43	7.31×10^{-4}	0.065	0.78
11	7.7	1 mM HEPES 3 mg/L Carbomer 3 mM NaCl	33	0.38	7.0	97	99	116	-38	2.78×10^{-4}	0.024	1.42
12	7.7	1 mM HEPES 3 mg/L Carbomer 3 mM NaCl	33	0.37	7.6	97	98	124	-39	2.81×10^{-4}	0.024	1.39

610 [a]Influent $nTiO_2$ concentration. [b]Pore-water velocity. [c]Average of influent particle diameter at beginning and end of pulse injection. [d]Attachment rate. [e]Attachment
611 efficiency. [f]Maximum retention capacity.

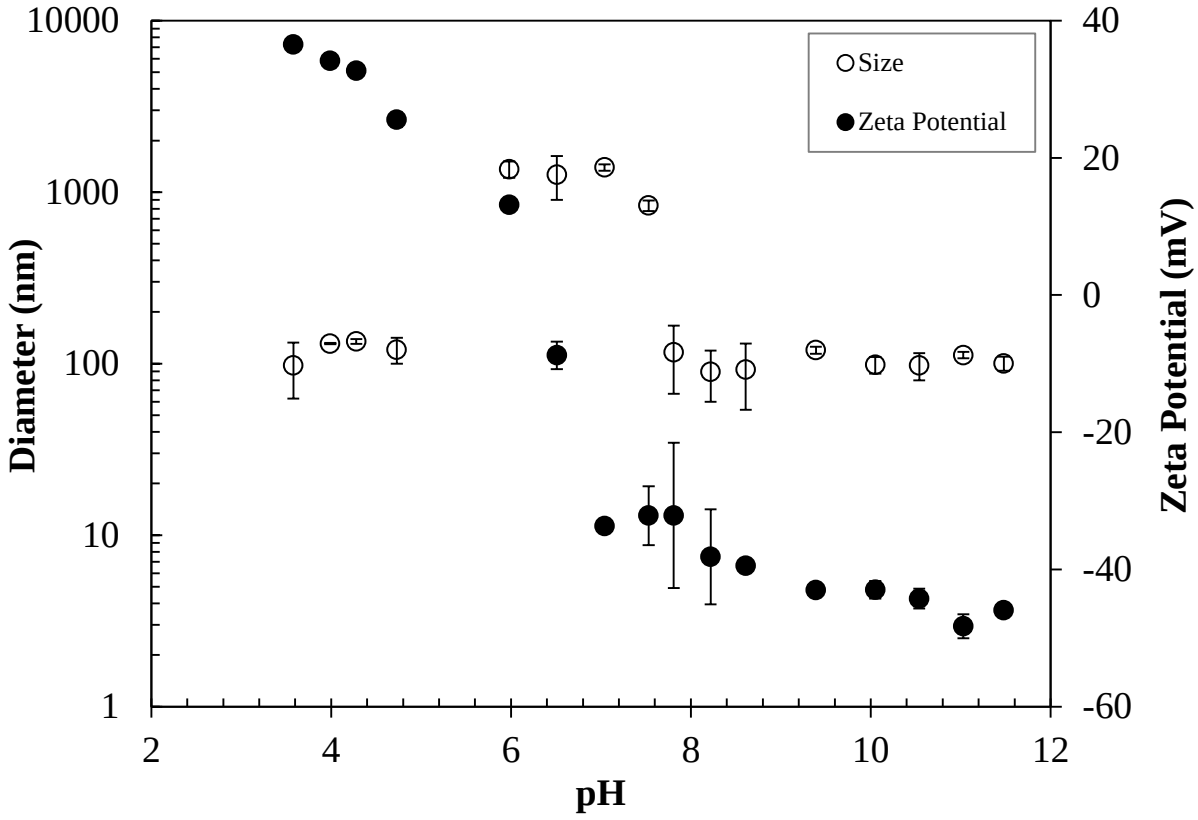

Figure 1. Effect of pH on $nTiO_2$ particle size and zeta potential in DI water. Error bars represent standard deviation of 3 replicate measurements.

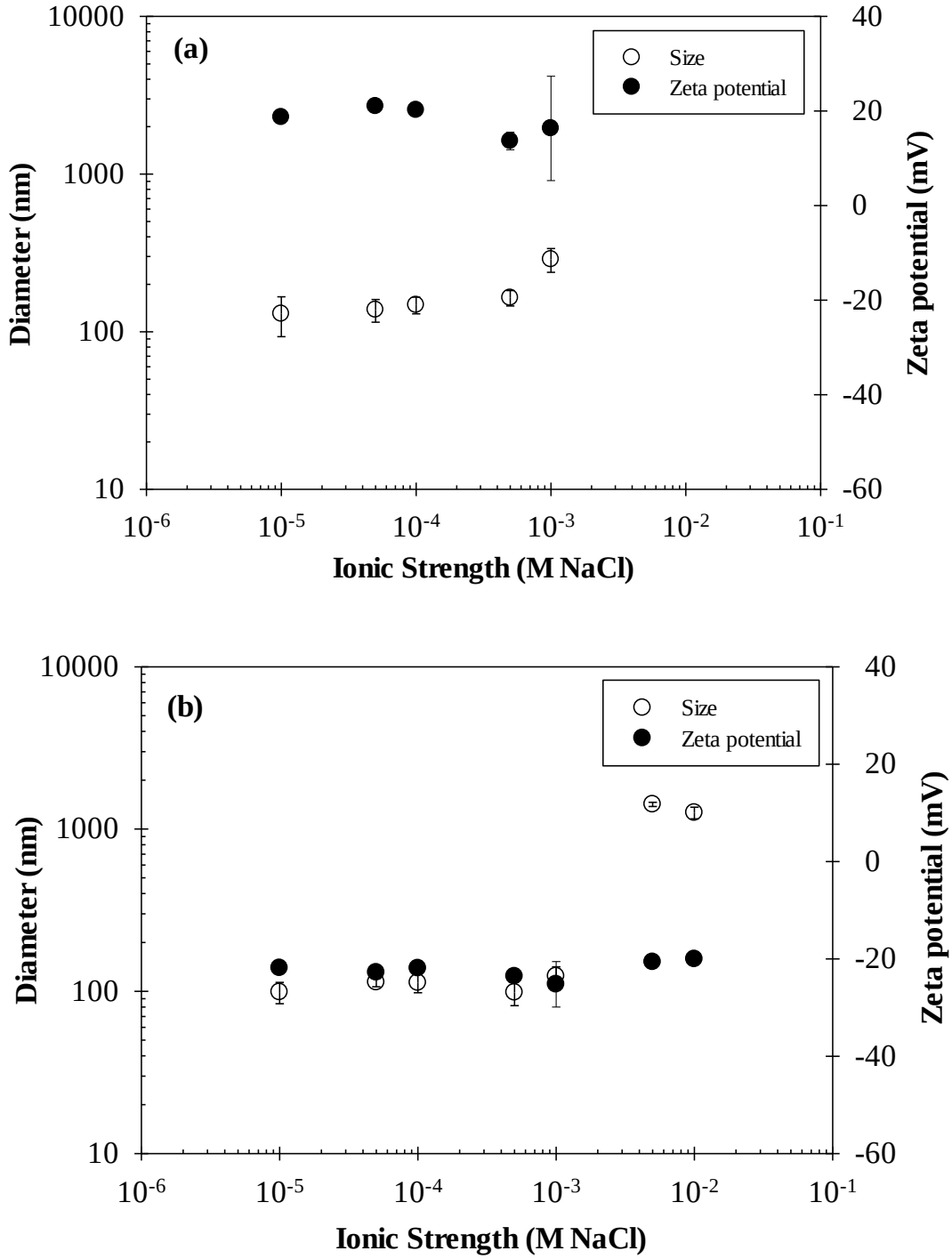

Figure 2. Effect of ionic strength (IS) on zeta potential and $nTiO_2$ particle size at (a) pH 5 and (b) pH 7.5. Error bars represent standard deviation of 3 replicate measurements. At pH 5 and ≥0.005 M NaCl, $nTiO_2$ suspensions became unstable, resulting in sedimentation of larger nanoparticle aggregates and unstable size and zeta potential readings.

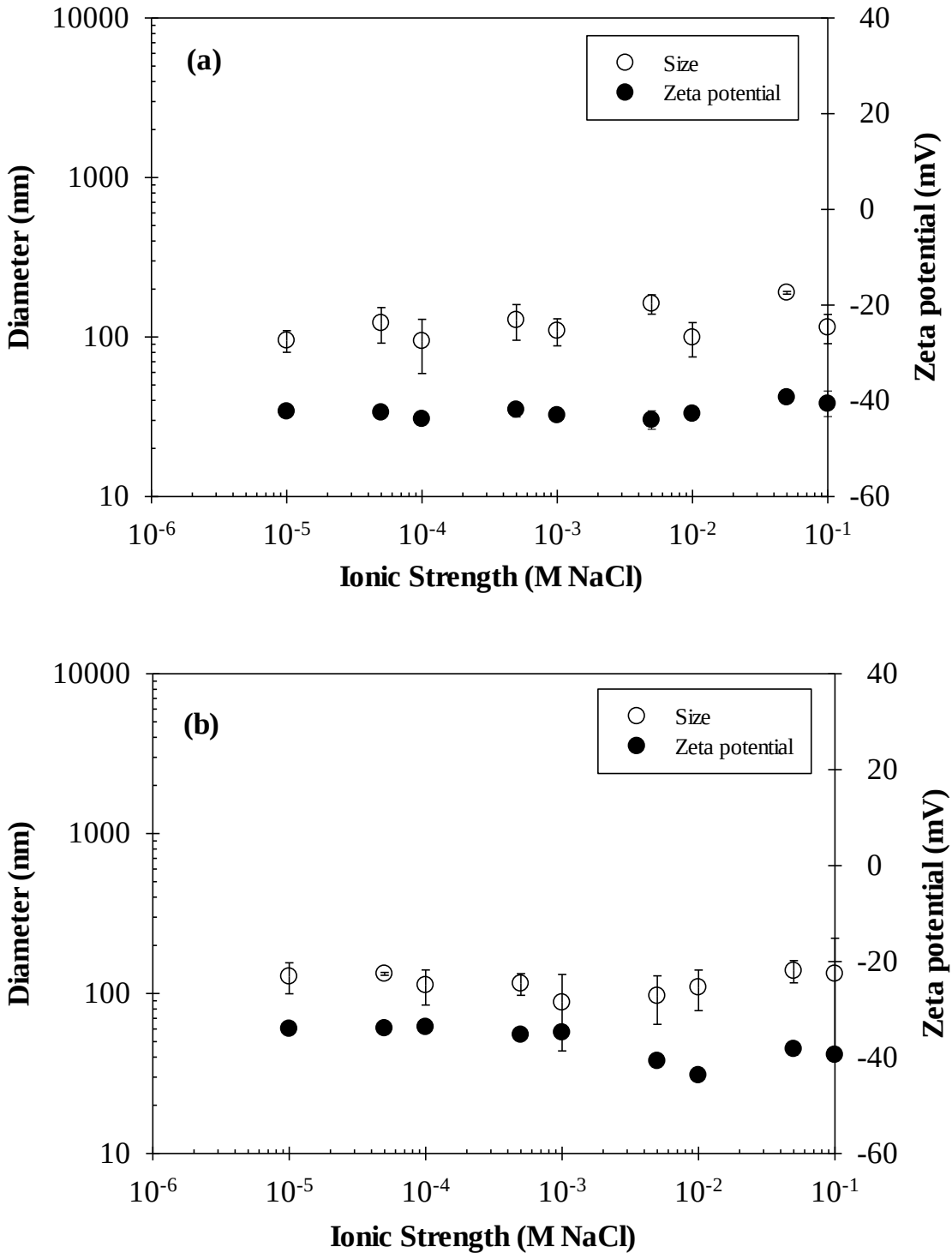

Figure 3. Effect of IS on zeta potential and $nTiO_2$ particle size in the presence of 3 mg/L Carbomer at (a) pH 5 and (b) pH 7.5. Error bars represent standard deviation of 3 replicate measurements.

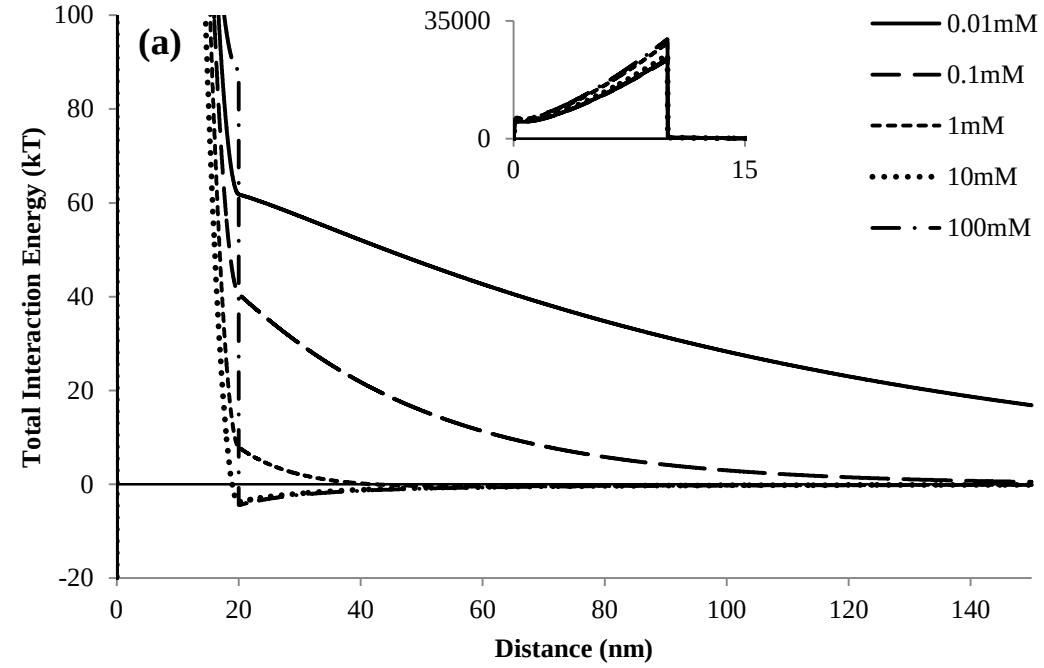

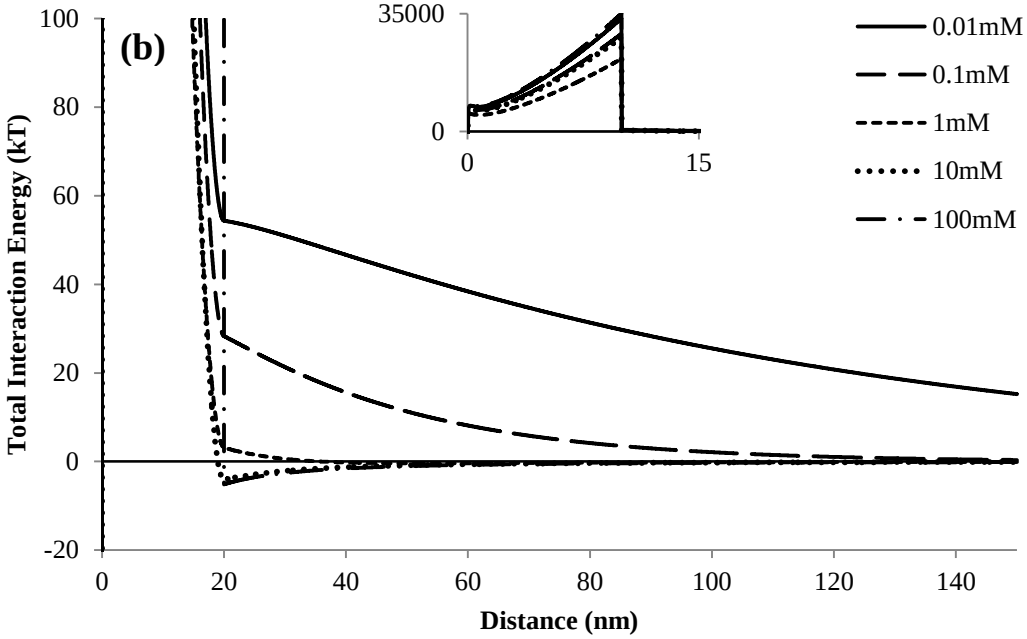

Figure 4. Interaction energy profiles obtained using XDLVO theory for two $nTiO_2$ particles in the presence of Carbomer at (a) pH 5 and (b) pH 7.5. Insets show the y-axis on a larger scale**.**

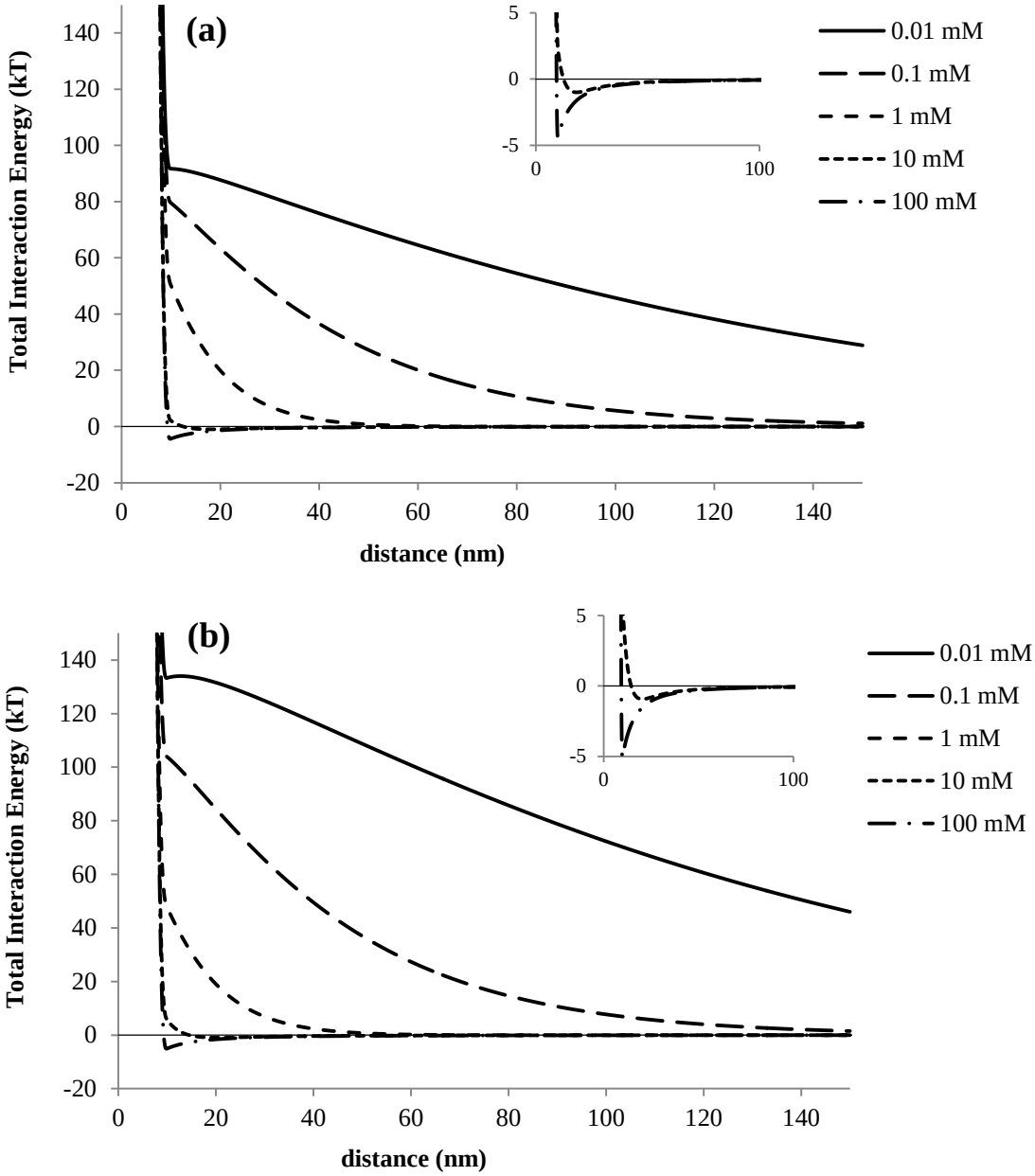

Figure 5. XDLVO interaction profiles for $nTiO_2$ and a quartz surface (i.e., sand grain) in the presence of Carbomer at (a) pH 5 and (b) pH 7.5. Inset shows secondary attractive energy minimum for IS ≥10 mM NaCl.

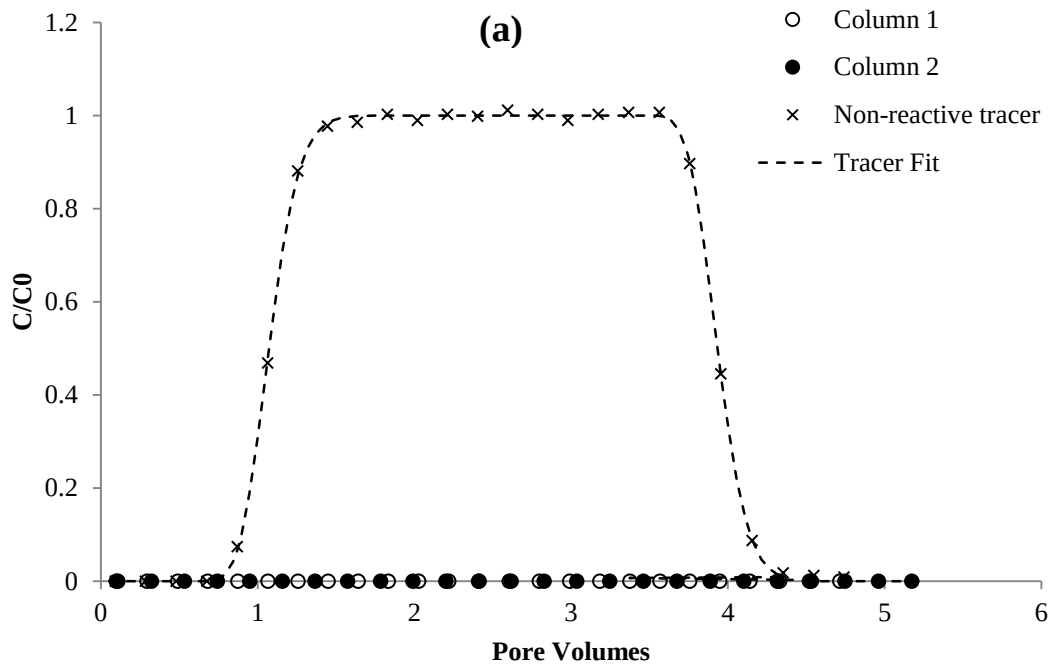

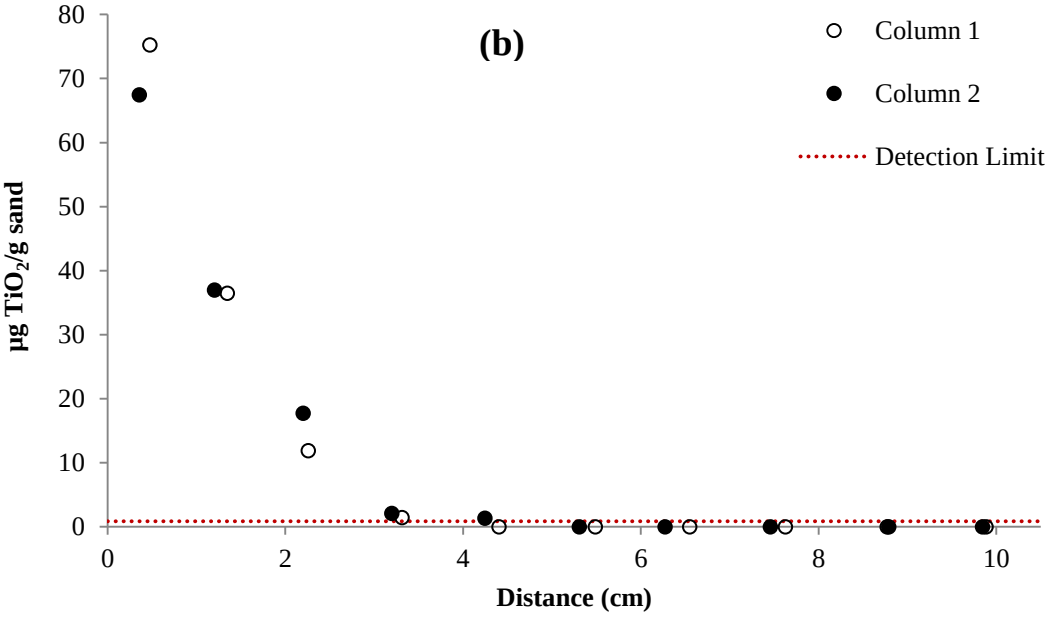

Figure 6. Experimentally measured (a) effluent breakthrough curves and (b) retention profiles obtained for $nTiO_2$ in Federal Fine (30-140 mesh) Ottawa sand at pH 5.0 without Carbomer (duplicate columns). The non-reactive tracer fit is shown in (a), from which the hydrodynamic dispersion coefficient (D_H) was calculated to be 0.056.

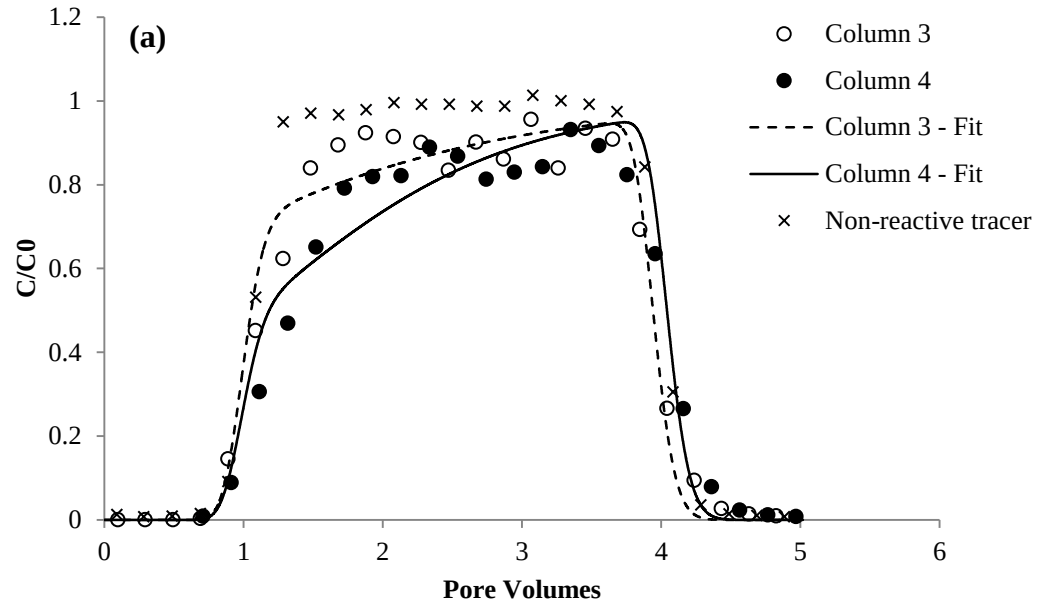

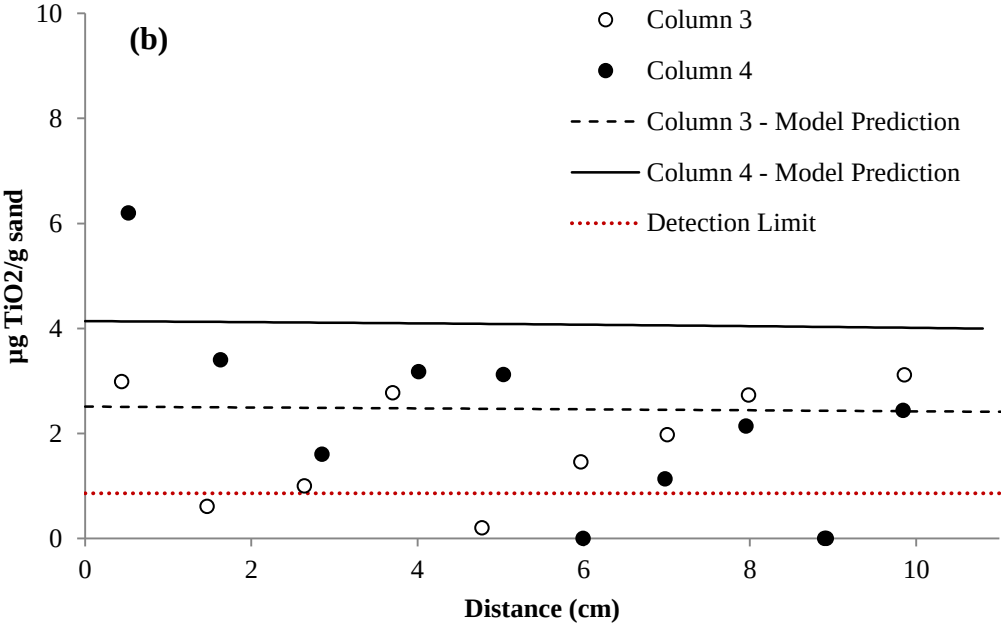

Figure 7. Comparison of experimentally measured and simulated (a) transport and (b) retention of $nTiO_2$ alone at pH 7.4 in Federal Fine (30-140 mesh) Ottawa sand (duplicate columns).

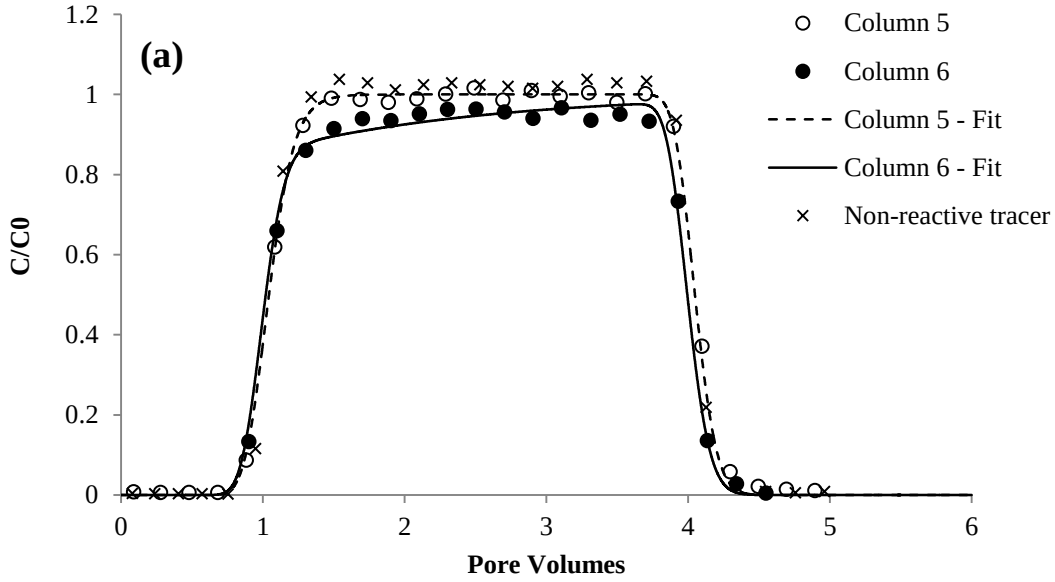

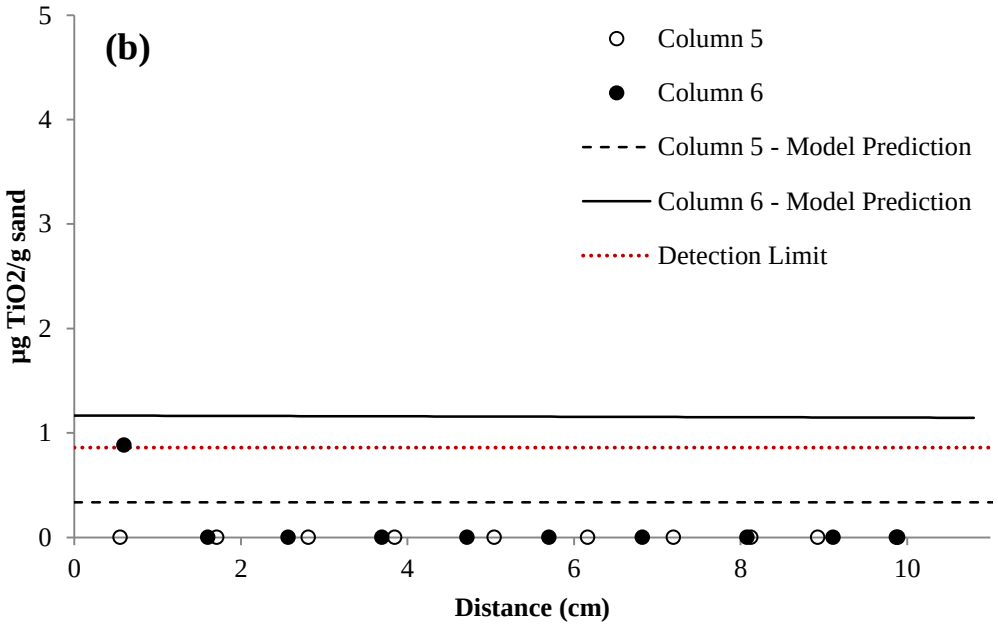

Figure 8. Comparison of experimentally measured and simulated (a) effluent breakthrough curves and (b) retention profiles for $nTiO_2$ with 3 mg/L Carbomer in Federal Fine (30-140 mesh) Ottawa sand at pH 5.1 (duplicate columns).

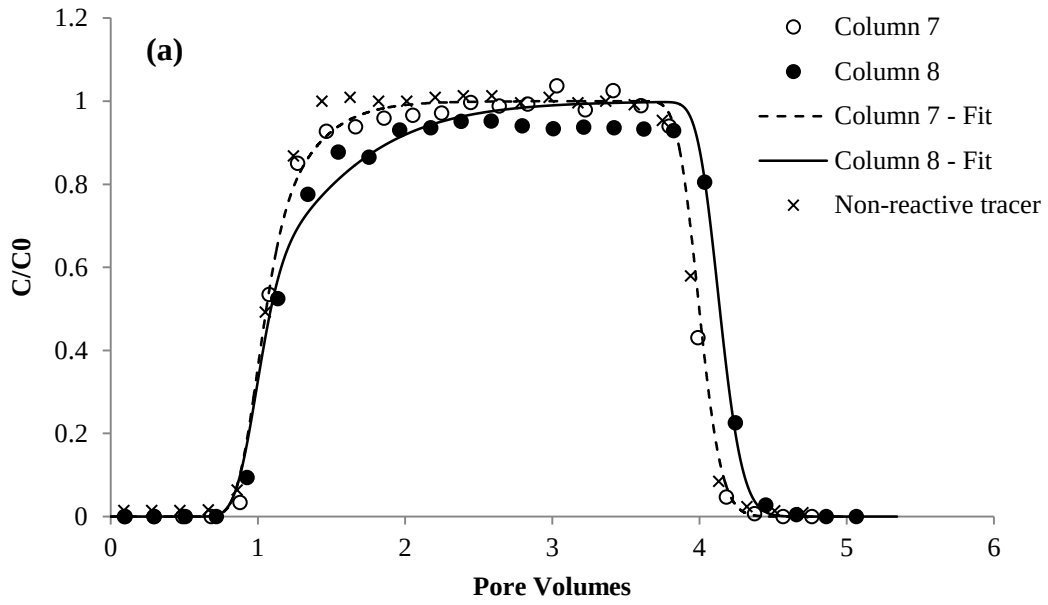

669

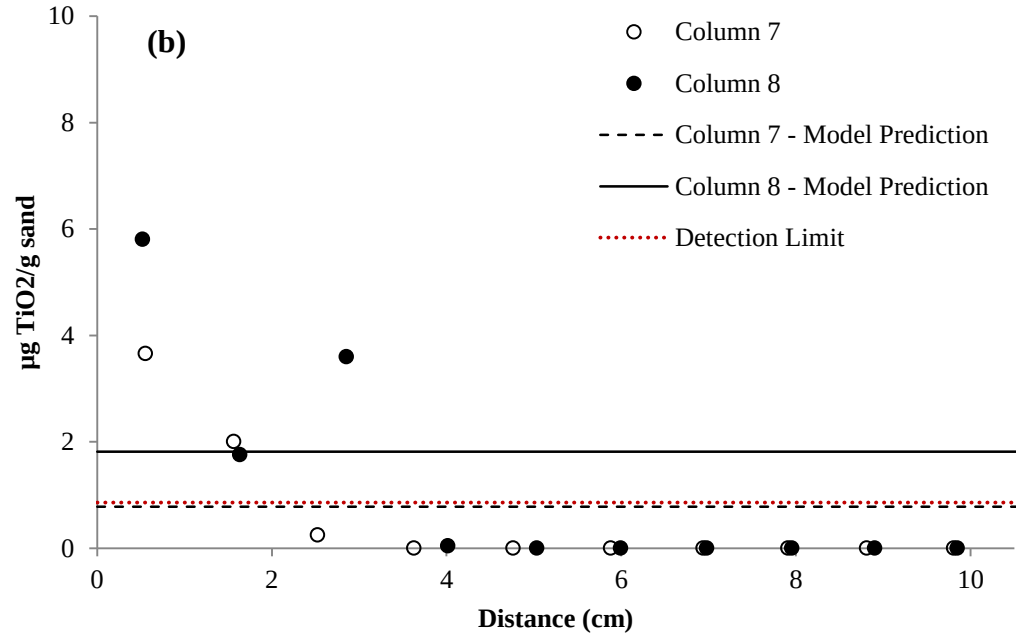

670

671 **Figure 9.** Comparison of experimentally measured and simulated (a) transport and (b) retention
672 of $nTiO_2$ with 3 mg/L Carbomer at pH 7.6 in Federal Fine (30-140 mesh) Ottawa sand (duplicate
673 columns).

674
675